Acta Cryst. (1998). A**54**, 172–185

Primary Extinction in Cylinders and Spheres

GUNNAR THORKILDSEN* AND HELGE B. LARSEN

Department of Mathematics and Natural Science, Stavanger College, Ullandhaug, 4004 Stavanger, Norway. E-mail: gunnar.thorkildsen@tn.his.no

(*Received 30 May 1997; accepted 22 September 1997*)

Abstract

By transforming the Takagi equations into a representation using angular coordinates, it is in principle possible to obtain analytical expressions for the coefficients in a series expansion for the primary extinction factor in perfect crystals with a circular diffraction plane. In practice, it has been possible to obtain the first five terms in the expansion. This involves establishing recurrence relations for the families of Bragg and Laue boundary-value Green functions combined with integrations over the entrance and exit surfaces. The calculations, which cover the whole range of values for the scattering angle, θ_{oh}, are performed using the mathematical software systems *Mathematica* and *Maple*.

1. Introduction

The attenuation of the diffracted intensity due to *coherent* multiple scattering within a crystal is denoted *primary extinction* (Darwin, 1914), whereas the intensity reduction caused by *incoherent* multiple scattering is known as *secondary extinction* (Darwin, 1922). One of the main difficulties when modelling extinction is to properly deal with a crystal of finite shape. The present work addresses just this point, emphasizing the mathematical treatment for a perfect crystal in the shape of a cylinder or a sphere.

Analytical expressions for the primary extinction factor exist for the case of a semi-infinite crystal plate. For Bragg geometry, the solution was found by Darwin (1922) and, following the development of the dynamical theory (Ewald, 1917; von Laue, 1932), Zachariasen derived the corresponding expression for Laue transmission (Zachariasen, 1945). Over the years, several authors have dealt with the problem of multiple scattering in spheres. Early works include Ekstein (1951), Weiss (1952) and Zachariasen (1963). A major development based on the Hamilton–Zachariasen (H–Z) intensity coupling equations (Hamilton, 1957; Zachariasen, 1967), hence mainly dealing with secondary extinction, is due to Becker & Coppens (1974*a*,*b*).

In the present work, we use the Takagi–Taupin (T–T) equations (Takagi, 1962, 1969; Taupin, 1964) to express the coupling of the amplitudes of the transmitted and diffracted plane wave fields in a perfect crystal. The effect of the boundary on the propagation of the waves leads to a *region structure* bounded by families of characteristics (Sommerfeld, 1949) within the finite crystal. For crystals with a convex outer shape, we will have both a Bragg and a Laue family of regions. This concept is important for obtaining all contributions to the diffracted wave field at a given exit point from the various parts of the crystal, and has been used by several authors: Werner and co-workers (Werner & Arrott, 1965; Werner *et al.*, 1966; Werner, 1974) investigated secondary extinction based on the H–Z equations, whereas Uragami (1969, 1970, 1971) treated primary extinction in a parallelepipedal crystal using the T–T equations. Uragami applied Riemann's method for dealing with hyperbolic partial differential equations, and obtained closed expressions for the diffracted fields. A review of mathematical techniques in solving the H–Z and the T–T equations is given by Werner and co-workers (Werner *et al.*, 1986). Olekhnovich & Olekhnovich pursued the ideas of Uragami and calculated numerical values for the primary extinction factor (Olekhnovich & Olekhnovich, 1978). Saka, Katagawa & Kato (1972*a*,*b*, 1973) considered and classified multiple diffraction for various scattering geometries. Further important advances concerning extinction in general were due to Kato (1976*a*,*b*), who later initiated the development of the statistical dynamical theory (Kato, 1980*a*,*b*,*c*). Kato (1976*a*) also derived a relation connecting the expressions for the integrated power in the case of an incident spherical wave (point source) and an incident plane wave. Becker and co-workers (Becker, 1977; Becker & Dunstetter, 1984) advocated the point-source concept and the series-expansion approach, devising a powerful theoretical foundation for treating primary extinction in finite crystals. In the present work, we closely follow the approach of Becker, with particular emphasis on a rigorous treatment of *all* region types. We will however not use integrations for an *extended* volume but explicitly perform the surface integrations of the intensity expressions for the field densities.

A problem in dealing with spherical geometry is the description of the circular boundary contour. The method of Uragami seems to be workable for crystals bounded by *plane surfaces* only. The direct extension of this work to a cylinder by Olekhnovich & Olekhnovich (1980) thus

implies, in our opinion, an indirect use of a quasi-circular boundary geometry. Authors like Kawamura & Kato (1983) and Al Haddad & Becker (1990) devised different schemes for approximating the circle by straight-line segments. In the present treatment, no approximations are made. The Takagi equations are expressed in angular variables, which make them suitable for dealing with boundary conditions along the circular contour.

In the first part of this paper, we establish the concept of *a generalized extinction factor* for a perfect crystal:† the coupled effect on the kinematical power due to multiple scattering, absorption and anomalous dispersion, *cf.* Becker (Becker & Coppens, 1974*a*; Becker, 1983), Härtwig (1987) and Batterman & Cole (1964). In the second part, we apply the general concepts to perfect cylindrical and spherical crystals. We here only consider the non-absorbing case. Absorption is treated separately in another paper (Thorkildsen & Larsen, 1998).

All calculations are performed symbolically using the mathematical software packages *Mathematica* Version 2.2.3 (Wolfram, 1991) and *Maple V* Release 3 (Char *et al.*, 1991*a*,*b*).

2. Generalized extinction factor

2.1. *The Takagi equations in the two-beam case*

The electric displacement field within the crystal is written as an Ewald wave, $\mathbf{D}(\mathbf{r})$, built of two plane-wave components, $\mathbf{D}_{\mathbf{k}_o}$ and $\mathbf{D}_{\mathbf{k}_h}$, representing the transmitted and diffracted wave fields, respectively:‡

$$\begin{aligned}\mathbf{D}(\mathbf{r}) &= \mathbf{D}_{\mathbf{k}_o} + \mathbf{D}_{\mathbf{k}_h} \\ &= \mathbf{D}_o(\mathbf{r})\exp(-2\pi i\mathbf{k}_o\cdot\mathbf{r}) + \mathbf{D}_h(\mathbf{r})\exp(-2\pi i\mathbf{k}_h\cdot\mathbf{r}).\end{aligned} \tag{1}$$

Combining Maxwell's equations for a dielectric medium (Jackson, 1975), using von Laue's approximation (von Laue, 1932) for the electric field:

$$\mathbf{E} \simeq (1/\epsilon_o)(1-\chi_e)\mathbf{D}$$

with a Fourier expansion of the electric susceptibility, $\chi_e(\mathbf{r})$, which is a periodic function in the Bravais lattice:

$$\chi_e(\mathbf{r}) = \sum_p \chi_p \exp(-2\pi i\mathbf{p}\cdot\mathbf{r}),$$

one obtains the Takagi equations (Takagi, 1962, 1969; Taupin, 1964), a set of partial differential equations for the amplitudes of the wave components in a perfect crystal. They are here written for one state of polarization (σ or π):

$$\partial D_o/\partial s_o = i\kappa_{oh}D_h \tag{2}$$

$$\partial D_h/\partial s_h = 2\pi i\beta_h D_h + i\kappa_{ho}D_o. \tag{3}$$

† Here expressed as a series expansion.

‡ The time-dependent factor $\exp(2\pi i\nu t)$ is omitted in the equations.

The equations are valid to first order in χ_o, the mean electrical susceptibility, which for X-rays has a value of the order of 10^{-5}. In the derivation, it is assumed that the magnitude of the spatial derivatives of D_p, $p \in \{o, h\}$, is of the same order as χ_o. s_o and s_h are spatial coordinates along the incident and the diffracted wave vector, $\mathbf{K}_o$ and $\mathbf{K}_h = \mathbf{K}_o + \mathbf{h}$, respectively. The corresponding unit vectors are denoted $\mathbf{s}_o$ and $\mathbf{s}_h$. They define the diffraction plane. $\mathbf{h}$ is a reciprocal-lattice vector. In this work, we will use $\mathbf{K}_p$ to represent wave vectors in vacuum and $\mathbf{k}_p$ to represent wave vectors within the crystal.

The deviation parameter, β_h, is defined by (Authier & Simon, 1968; Authier, 1996*b*) (*cf.* Fig. 1)

$$\beta_h \overset{\text{def}}{=} \|\mathbf{k}_h\| - k$$

and the coupling parameter, κ_{pq}, by

$$\kappa_{pq} = -\pi KC\chi_{p-q} = (r_e\lambda C/V_c)F_{p-q}. \tag{4}$$

r_e is the classical electron radius, λ is the wavelength of the incident radiation, C is the actual polarization factor, V_c is the volume of the unit cell and F_{p-q} is the structure factor associated with the reciprocal-lattice point $p-q$.

The first term on the right-hand side of (3) may be eliminated by the transformation

$$D_p = \tilde{D}_p \exp(2\pi i\beta_h s_h) \tag{5}$$

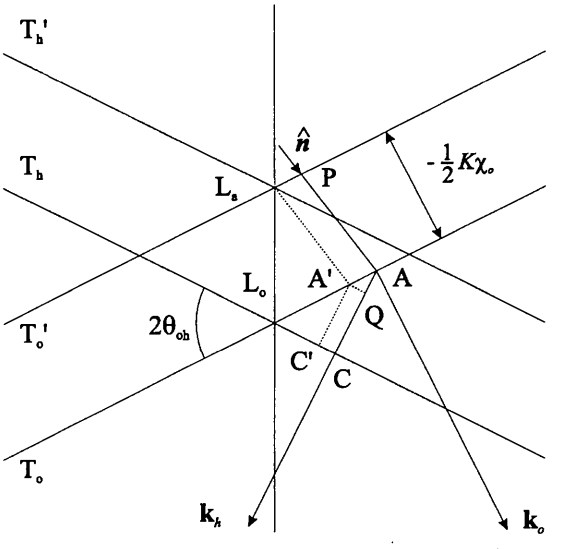

Fig. 1. Illustration of the 'dispersion' surface in a two-beam Takagi case. $L_aP = -K\Delta\theta_{oh}$, $L_aA' = -K\chi_o/2\gamma_o$, $A'C' = -\frac{1}{2}K\chi_o(1-\gamma_h/\gamma_o)$ and $AC = \|\mathbf{k}_h\| - k = \beta_h$. $AQ = \alpha_h = \|\mathbf{K}_h\| - K$. L_a denotes the Laue point and L_o the Lorentz point. PA is the *Anpassung*. $\hat{\mathbf{n}}$ is a unit vector normal to the crystal surface. $\gamma_o = \hat{\mathbf{n}}\cdot\mathbf{s}_o$ and $\gamma_h = \hat{\mathbf{n}}\cdot\mathbf{s}_h$. T'_o and T'_h are parts of the circles drawn from the respective reciprocal-lattice points o and h with radius $K = 1/\lambda$, which is the vacuum wave number. T_o and T_h are drawn with radius $k = K(1+\frac{1}{2}\chi_o)$, the wave number within the crystal.

and we arrive at

$$\partial\tilde{D}_o/\partial s_o = i\kappa_{oh}\tilde{D}_h \tag{6}$$

$$\partial\tilde{D}_h/\partial s_h = i\kappa_{ho}\tilde{D}_o. \tag{7}$$

These coupled equations are the starting point for obtaining the generalized extinction factor in a perfect crystal. They can be combined to give two second-order hyperbolic partial differential equations. The equation for the amplitude of the diffracted wave is for instance given by

$$\partial^2\tilde{D}_h/\partial s_o\partial s_h + \kappa_{ho}\kappa_{oh}\tilde{D}_h = 0.$$

2.2. *Boundary conditions*

The wave field inside the crystal is induced by an incoming plane wave with wave vector $\mathbf{K}_o$. The *Anpassung*, *i.e.* the change of this wave vector, as the beam enters the crystal will be along the inward normal vector to the crystal surface (Pinsker, 1978; Authier, 1996*a*). This kinematical boundary condition is most easily depicted using the dispersion-surface concept of standard dynamical theory, *cf.* Fig. 1. It follows that $\beta_o \overset{\text{def}}{=} 0$.

Owing to the small value of χ_o, the exact boundary conditions for the fields, continuity of $\mathbf{D}_\perp$ and $\mathbf{E}_\parallel$ across the entrance surface (Jackson, 1975) are replaced by the condition of continuity of $\mathbf{D}$. Thus, at the point S at the entrance surface, *cf.* Fig. 2, we have

$$D_o^{(b)}(S)\exp[-2\pi i\mathbf{k}_o\cdot\mathbf{r}(S)] = D_o^{(e)}(S)\exp[-2\pi i\mathbf{K}_o\cdot\mathbf{r}(S)].$$

For the transformed field, $\tilde{D}_o$, we then get†

$$\tilde{D}_o^{(b)}(S) = D_o^{(e)}(S)\exp[-2\pi i\alpha_h s_h(S)] \times \exp\{\pi i K\chi_o[s_o(S)+s_h(S)]\}. \tag{8}$$

† The superscript (b) is used to indicate a boundary point.

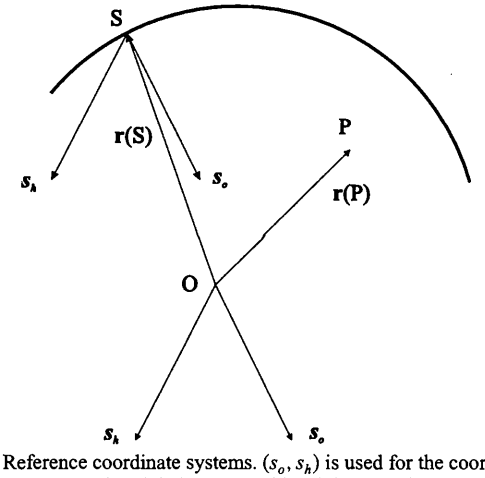

Fig. 2. Reference coordinate systems. (s_o, s_h) is used for the coordinates with respect to the global system with origin at O. (Δ_o, Δ_h) is used for the coordinates with respect to the local system with origin at S.

α_h is the *excitation error*:

$$\alpha_h = -K\,\Delta\theta_{oh}\sin 2\theta_{oh}.$$

$\Delta\theta_{oh}$ is the departure angle from Bragg's law. $\Re\chi_o$ and $\Im\chi_o$, the real and imaginary parts of the mean electrical susceptibility, will determine the refraction and absorption of the X-rays. To keep track of the changes in the wave vectors due to these effects, we explicitly express the diffracted wave at the point P within the crystal by

$$\begin{aligned} D_{\mathbf{k}_h}(P) &= D_h(P)\exp[-2\pi i\mathbf{k}_h\cdot\mathbf{r}(P)] \\ &= \tilde{D}_h(P)\exp[-2\pi i\mathbf{K}_h\cdot\mathbf{r}(P)]\exp[2\pi i\alpha_h s_h(P)] \\ &\quad\times\exp\{-\pi iK\chi_o[s_o(P)+s_h(P)]\}. \end{aligned} \tag{9}$$

2.3. *Method of solution*

Using the method of Riemann for solving hyperbolic partial differential equations (Sommerfeld, 1949; Sneddon, 1957; Authier & Simon, 1968; Takagi, 1969), the diffracted wave field at the point P is found by a path integral, *cf.* Fig. 3.

$$\tilde{D}_h(P) = (i\kappa_{ho}/\sin 2\theta_{oh})\int_A^B \mathbf{s}_o\cdot\mathrm{d}\mathbf{S}\,G_h(P|S)\tilde{D}_o^{(b)}(S). \tag{10}$$

$\mathrm{d}S$ is a curvilinear coordinate in the diffraction plane along the entrance contour. $\mathrm{d}\mathbf{S} = \hat{\mathbf{n}}\,\mathrm{d}S$, with $\hat{\mathbf{n}}$ being the inward unit normal vector to the contour at S. $i\kappa_{ho}G_h$ is the boundary-value Green function, which is the solution of the Takagi equations for the diffracted field, subject to the boundary condition

$$\tilde{D}_o^{(b)}(S) = \delta(s_h - s_h(S)). \tag{11}$$

The use of a Dirac δ function in the boundary condition leads to the concept of a *point source*. In principle, one should include the factor $\delta(z - z(S))$ and speak of a field density. z is a coordinate perpendicular to the diffraction plane. An integration along z selects the diffraction plane associated with S. We may thus speak of an integration over the entrance surface. In general, $G_h(P|S) = G_h(\Delta_o, \Delta_h)$ with $\Delta_o = s_o(P) - s_o(S)$ and $\Delta_h = s_h(P) - s_h(S)$. Having an incoming *plane wave* with

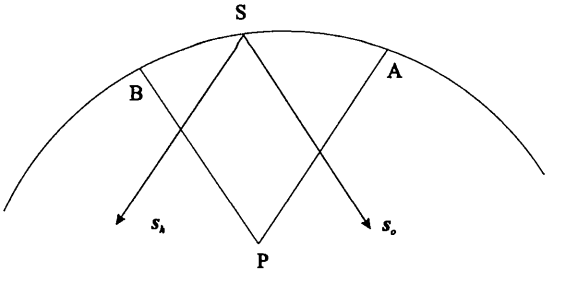

Fig. 3. Range of integration (A, B) associated with the interior point P. *BPA* represents the so called Borrmann triangle.

constant amplitude, $D_o^{(e)}$, we find† for the diffracted wave at P:

$$D_{\mathbf{k}_h}(P) = (i\kappa_{ho}D_o^{(e)}/\sin 2\theta_{oh}) \int_{S(P)} \mathbf{s}_o \cdot \mathrm{d}\mathbf{S}\, G_h(\Delta_o, \Delta_h) \times \exp(2\pi i\alpha_h \Delta_h) \exp[-\pi i K \chi_o(\Delta_o + \Delta_h)]. \quad (12)$$

We have used the notation $S(P)$ to denote that part of the entrance surface where source points can contribute to the diffracted wave field at P.

2.4. *Generalized extinction factor for a perfect crystal*

The integrated diffracted power, $\mathcal{P}_h$, in the case of an incoming plane wave is obtained by a two-step procedure:

(i) Moving the general point P to a point M on the exit boundary. The power is obtained by integrating across the exit surface (Kato, 1976*a*; Becker, 1977):

$$P_h = \int \mathrm{d}z \int_M \mathbf{s}_h \cdot \mathrm{d}\mathbf{M}\, |D_{\mathbf{k}_h}|^2.$$

The range of integration in z now spans the vertical dimension of the exit surface of the crystal.

(ii) Integrating the power across $\varepsilon = \Delta\theta_{oh}$, the glancing angle of the incident beam with respect to the scattering plane (Zachariasen, 1945; Kato, 1980*d*):

$$\mathcal{P}_h = \int_{-\infty}^{\infty} \mathrm{d}\varepsilon\, P_h(\varepsilon).$$

The result is

$$\mathcal{P}_h = \mathcal{P}_h^{(0)}(1/v \sin 2\theta_{oh}) \int \mathrm{d}z \int_M \mathbf{s}_h \cdot \mathrm{d}\mathbf{M} \int_{S(M)} \mathbf{s}_o \cdot \mathrm{d}\mathbf{S} \times |G_h(\Delta_o, \Delta_h)|^2 \exp[-\mu(\Delta_o + \Delta_h)], \quad (13)$$

where $\mathcal{P}_h^{(0)}$ is the kinematical integrated power. v is the volume of the crystal and $\mu = -2\pi K \Im\chi_o$ is the linear absorption coefficient.

The generalized extinction factor, y, for a perfect crystal is defined by

$$y = \mathcal{P}_h/\mathcal{P}_h^{(0)}.$$

In the general case of a convex crystal, the effect of the boundary leads to a set of Green functions, each one related to a specific region of the crystal. The regions are obtained by a ray-tracing procedure, which draws the characteristics with origin at the source point S. This divides the crystal into the various parts, m. The division depends on the position of S on the entrance surface and the crystal and scattering geometry. In fact, there will be two families of Green functions:‡ a Bragg family (r = B) when $\gamma_h < 0$, *cf.* Fig. 9, and a Laue family (r = L) when $\gamma_h > 0$, *cf.* Fig. 11. γ_h is defined in Fig. 1. We denote the families of boundary-value Green functions by $\{G_h(\Delta_o, \Delta_h|m; r)\}$. The generalized extinction factor is then expressed by

$$y = (1/v \sin 2\theta_{oh}) \sum_r \sum_{m=m'(r)} \int \mathrm{d}z \int_{M(m)} \mathbf{s}_h \cdot \mathrm{d}\mathbf{M} \int_{S(M)} \mathbf{s}_o \cdot \mathrm{d}\mathbf{S} \times |G_h(\Delta_o, \Delta_h|m; r)|^2 \exp[-\mu(\Delta_o + \Delta_h)]. \quad (14)$$

The sums cover both families and all the regions m' that have their boundaries along the exit surface.

It has been shown in the literature (Becker, 1977) that the surface integrations can be transformed to a volume integration for an extended volume v':

$$(1/\sin 2\theta_{oh}) \sum_r \sum_{m=m'(r)} \int \mathrm{d}z \int_{M(m)} \mathbf{s}_h \cdot \mathrm{d}\mathbf{M} \int_{S(M)} \mathbf{s}_o \cdot \mathrm{d}\mathbf{S} = \int_{v'} \mathrm{d}V = v'.$$

In this work, we will explicitly carry out the surface integrations. The actual result for the extended volume is used as a check for the integration setup.

Performing the symbolic expansion

$$|G_h(\Delta_o, \Delta_h|m; r)|^2 = \sum_{n=0}^{\infty} (-1)^n |u|^n I_h^{(n)}(\Delta_o, \Delta_h; \Phi|m; r) \quad (15)$$

with the parameter u defined by

$$u = \kappa_{oh}\kappa_{ho}\ell^2. \quad (16)$$

$\ell = \ell(z)$ (a real number) is a characteristic length parameter of the scattering system. Taking anomalous scattering into account, u is a complex quantity:

$$u = |u| \exp(i\Phi)$$

with

$$\Phi \overset{\text{def}}{=} \varphi_{oh} + \varphi_{ho},$$

$$|u| = (\ell/\Lambda_{oh})^2,$$

φ_{pq} is the phase of κ_{pq} or equivalently the phase of the structure factor F_{p-q}. Λ_{oh} is an extinction length.

$$\Lambda_{oh} \overset{\text{def}}{=} |\kappa_{oh}\kappa_{ho}|^{-1/2}.$$

It then follows, *cf.* (14) and (15), that the generalized extinction factor, y, depends upon:

(i) Crystal geometry/scattering condition – through ℓ/Λ_{oh}, the actual region structure (m; r) and the surface integration setup (z, $M(m')$, $S(M)$).

(ii) Normal absorption – through μ.

(iii) Anomalous scattering – through Φ.

With μ and Φ put to zero, we will denote the generalized extinction factor as the extinction factor for perfect crystals, symbolized by y_p.

† The carrier wave $\exp[-2\pi i\mathbf{K}_h \cdot \mathbf{r}(P)]$ is omitted in (12). It will not influence the *intensity* of the diffracted beam at P.

‡ Corresponding to the Bragg–(Bragg)$^{2n(+1)}$ and Laue–(Bragg)$^{2n(+1)}$ classification of Saka *et al.* (1972*a*,*b*, 1973).

The main challenges to obtain analytical results for the generalized extinction factor are:

(i) Obtain the Green functions, $G_h(\Delta_o, \Delta_h|m; r)$, either in closed form or as series expansions.

(ii) Establish the algorithms for the integration setup, *i.e.* the connected limits $\{M(m'), S(M)\}$ for the Bragg and Laue cases.

These are two general points, which have to be addressed for any given crystal shape.

3. Crystals with a diffraction plane in the shape of a circle

3.1. *Geometry and coordinates*

A point in the diffraction plane is represented by the spatial coordinates (Δ_o, Δ_h) measured with respect to a local coordinate system with origin at the source point S. As a global coordinate system, we here use (x, y) with $-x$ along the reciprocal-lattice vector of the atomic scattering planes and the origin O at the centre of the circular diffraction plane. The positions of S and the exit point M are measured by the angles ψ_S and ψ_M between the x axis and the radius vectors $\overrightarrow{OS}$ and $\overrightarrow{OM}$, respectively, *cf.* Fig. 4.

A convenient angular representation, (φ_o, φ_h), of an interior point is found by drawing lines parallel to $\mathbf{s}_o$ and $\mathbf{s}_h$, in the opposite direction to the interceptions, N_o and N_h, with the circle contour, and measure the angles between the reference axes $\boldsymbol{\tau}_o$ and $\boldsymbol{\tau}_h$ and the radius vectors to the peripheral points. $\boldsymbol{\tau}_o$ is perpendicular to $\mathbf{s}_h$ and $\boldsymbol{\tau}_h$ is perpendicular to $\mathbf{s}_o$. Thus, $\varphi_o = \angle(\boldsymbol{\tau}_o, \overrightarrow{ON}_h)$ and $\varphi_h = \angle(\boldsymbol{\tau}_h, \overrightarrow{ON}_o)$. This is illustrated in Fig. 5.

The division into entrance and exit surfaces is shown in Fig. 6. It follows that the entrance surface is defined for

$$\psi_S \in (\theta_{oh}, \theta_{oh} + \pi) \tag{17}$$

with a subdivision into A and B parts. While the exit surface is given by

$$\psi_M \in (\pi - \theta_{oh}, 2\pi - \theta_{oh}), \tag{18}$$

which is built by the A and D parts. Following the notation of Saka *et al.* (1972*a*), *A–A* scattering, source point S and exit point M both positioned on A, will be denoted as Bragg–Bragg scattering, while the *B–D* situation will lead to Laue–Laue scattering. Similarly, the cases *A–D* and *B–A* are classified as Bragg–Laue and Laue–Bragg scattering, respectively.

The relations between the spatial and angular coordinates are in general given by

$$\cos\varphi_o = \cos(\psi_S + \theta_{oh}) + (\Delta_o \sin 2\theta_{oh}/R) \tag{19}$$

$$\cos\varphi_h = \cos(\psi_S - \theta_{oh}) - (\Delta_h \sin 2\theta_{oh}/R). \tag{20}$$

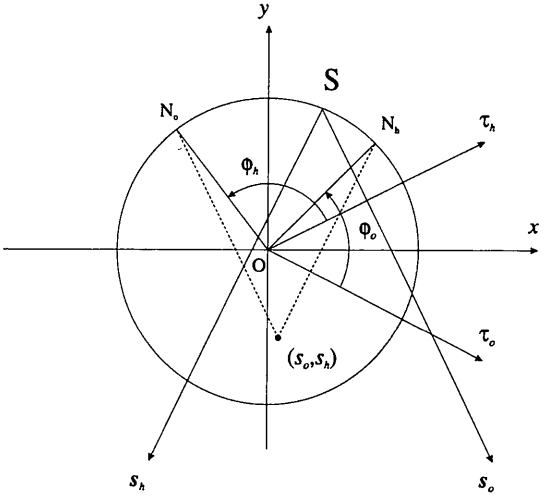

Fig. 5. Definitions of angular coordinates φ_o and φ_h for an interior point.

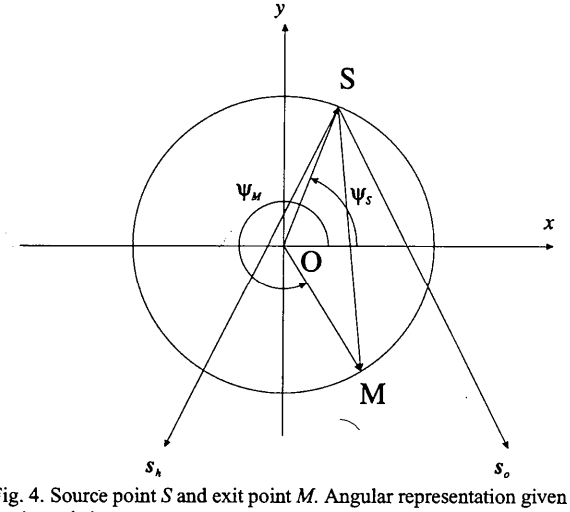

Fig. 4. Source point S and exit point M. Angular representation given by ψ_S and ψ_M.

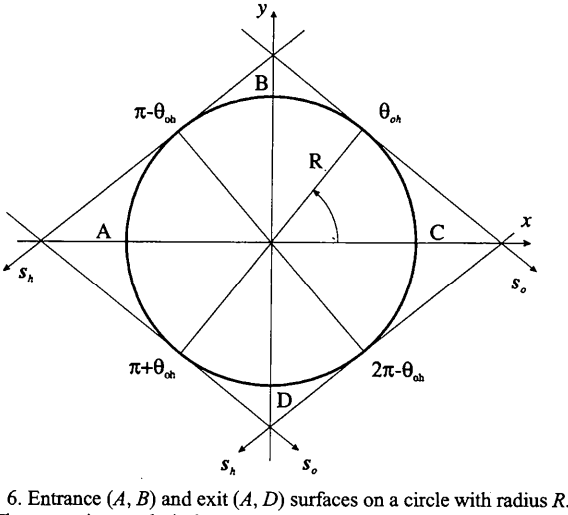

Fig. 6. Entrance (A, B) and exit (A, D) surfaces on a circle with radius R. The scattering angle is $2\theta_{oh}$.

For a point on the exit surface, *cf.* Fig. 7, we have

$$\varphi_o(M) = 2\pi - (\psi_M + \theta_{oh}) \tag{21}$$

$$\varphi_h(M) = \begin{cases} 2\pi - (\psi_M - \theta_{oh}) & M \text{ on } D \\ \psi_M - \theta_{oh} & M \text{ on } A \end{cases} \tag{22}$$

and consequently

$$\Delta_o(M) + \Delta_h(M) = R[(\sin\psi_S - \sin\psi_M)/\cos\theta_{oh}]. \tag{23}$$

It follows that the scalar product between the surface element $\mathrm{d}\mathbf{S}$ and the incident-beam direction $\mathbf{s}_o$ is

$$\mathrm{d}\mathbf{S} \cdot \mathbf{s}_o = \sin(\psi_S - \theta_{oh}) R \, \mathrm{d}\psi_S \tag{24}$$

while the scalar product between a surface element $\mathrm{d}\mathbf{M}$ of the exit surface, directed along the outward normal, and the diffracted-beam direction $\mathbf{s}_h$ becomes

$$\mathrm{d}\mathbf{M} \cdot \mathbf{s}_h = -\sin(\psi_M + \theta_{oh}) R \, \mathrm{d}\psi_M. \tag{25}$$

The extended volume, v', is shown in Fig. 8. It is here represented as an extended area in the diffraction plane and has a magnitude of

$$v' = [(\pi - \theta_{oh}) + \tan\theta_{oh}]R^2. \tag{26}$$

3.2. *The Takagi equations in angular coordinates*

By defining

$$\ell = R/\sin 2\theta_{oh},$$

we can express the Takagi equations using the angular coordinates (φ_o, φ_h) as

$$\partial\tilde{D}_o/\partial\varphi_o = -i\kappa_{oh}\ell \sin\varphi_o \tilde{D}_h \tag{27}$$

$$\partial\tilde{D}_h/\partial\varphi_h = \; i\kappa_{ho}\ell \sin\varphi_h \tilde{D}_o. \tag{28}$$

The boundary condition used to calculate the family of Green functions† is then given by

$$\tilde{D}_o^{(b)}(S) = [1/\ell \sin(\psi_S - \theta_{oh})]\delta(\varphi_h - (\psi_S - \theta_{oh})). \tag{29}$$

It turns out that the generalized extinction factor can be expressed‡ by [*cf.* (14)]

† The Green functions at the exit surface are now expressed by the angular variables ψ_S and ψ_M, *cf.* equations (19)–(22).

‡ $R \to R(z)$, the radius of the diffraction plane, in the general case. $R(z) = R$ for a cylinder.

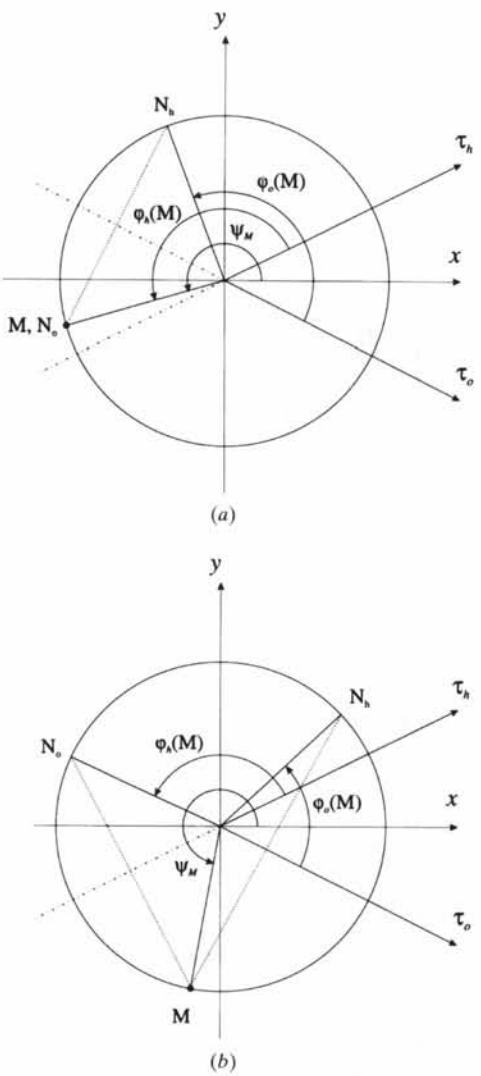

Fig. 7. Angular coordinates $\varphi_o(M)$ and $\varphi_h(M)$ for an exit point M. (*a*) M on part A of the exit surface. (*b*) M on part D of the exit surface.

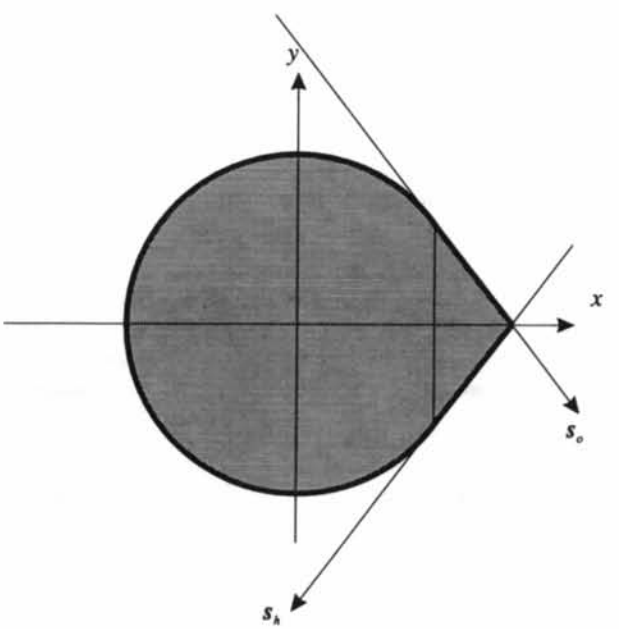

Fig. 8. Extended volume v' for a crystal in the shape of a cylinder.

$$y = (1/\pi \sin 2\theta_{oh}) \sum_r \sum_{m=m'(r)} \int_0^1 dz f(z) \times \int_{M(m)} d\psi_M [-\sin(\psi_M + \theta_{oh})] \times \int_{S(M)} d\psi_S \sin(\psi_S - \theta_{oh}) |G_h(\psi_S, \psi_M | m; r)|^2 \times \exp[-\mu R(z)(\sin\psi_S - \sin\psi_M)/\cos\theta_{oh}]. \quad (30)$$

$f(z)$ is a shape function. $f(z) = 1$ in the case of a cylinder and $f(z) = \frac{3}{2}(1 - z^2)$ in the case of a sphere. z is now treated as a dimensionless coordinate.

3.3. *Region structure*

3.3.1. *Source on entrance surface A – Bragg family.* When the source point S is on the A part of the entrance surface, the crystal is divided into regions as shown in Fig. 9 (*cf.* Uragami, 1971; Becker & Dunstetter, 1984). The number of regions that has to be taken into account will depend upon the value of the scattering angle $2\theta_{oh}$. This point will be discussed later. The boundary points,† φ_o^b and φ_h^b, associated with the interior point (φ_o, φ_h), will be at the crystal surface, φ^S, or at a border line, φ^B, between two regions. This has been visualized in Fig. 10 for the two classes of regions $m = 2p + 1$ and $m = 2p + 2$, where $p = 0, 1, \ldots$.

A careful geometrical analysis (Thorkildsen & Larsen, 1997*a*) gives the following equations for these points:

$$\begin{aligned} \varphi_o^B(p+1) &= 2\theta_{oh} - \varphi_h^B(p) && p \geq 0 \\ \varphi_h^B(0) &= \psi_S - \theta_{oh} \\ \varphi_h^B(p) &= 2\pi - 2\theta_{oh} - \varphi_o^B(p) && p \geq 1 \\ \varphi_o^S &= 2\pi - \varphi_h - 2\theta_{oh} \\ \varphi_h^S &= 2\theta_{oh} - \varphi_o. \end{aligned} \quad (31)$$

† The lower limits in the integration of the Takagi equations, *cf.* §3.4.

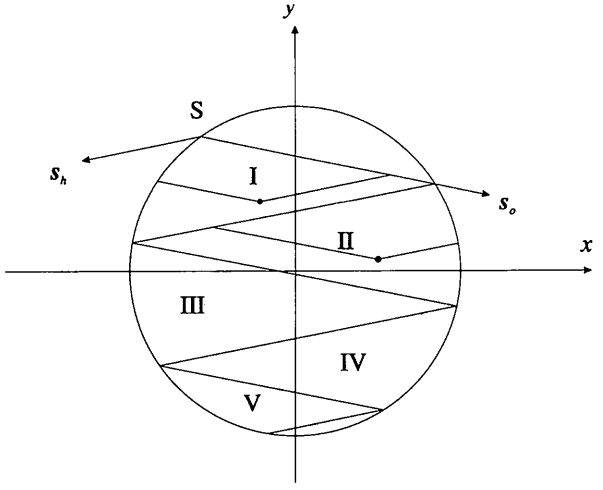

Fig. 9. Source point S on part A of the entrance surface. Division of the circular area into regions. Bragg case. Regions counted by Roman numbers.

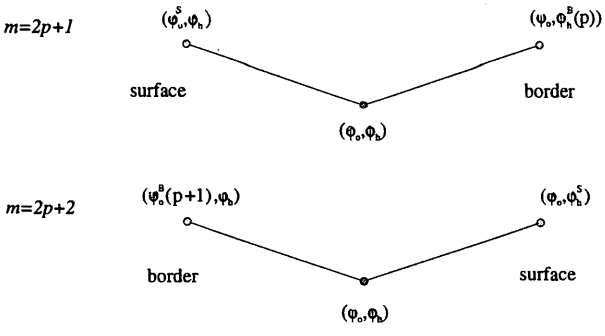

Fig. 10. Limits of integration for the integral operators – Bragg case.

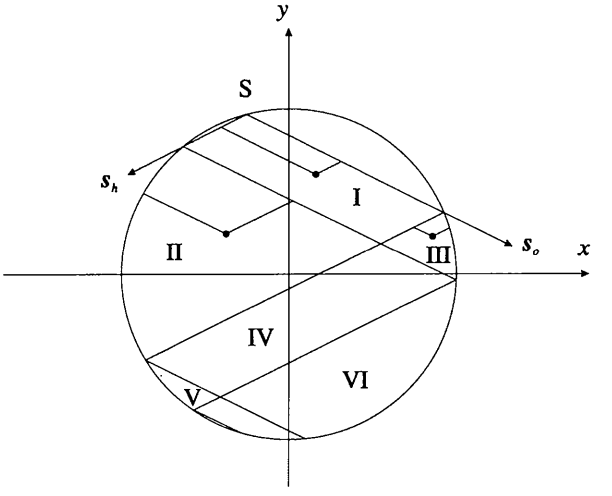

Fig. 11. Source point S on part B of the entrance surface. Region structure – Laue case.

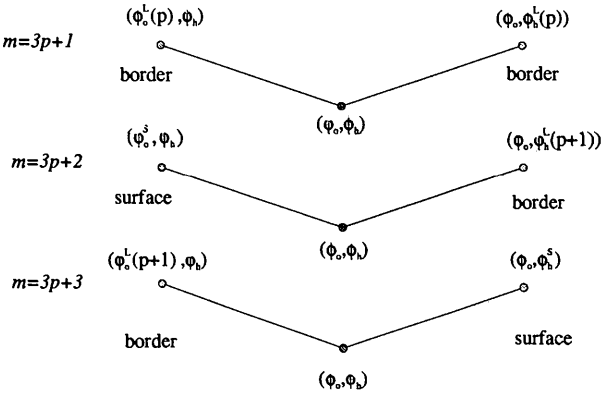

Fig. 12. Limits of integration for the integral operators – Laue case.

3.3.2. *Source on entrance surface B – Laue family.* When the source point S is on the B part of the entrance surface, the crystal is divided into regions as shown in Fig. 11. The boundary points for the three classes of regions, $m = 3p+1$, $m = 3p+2$ and $m = 3p+3$, $p = 0, 1, \ldots$, are schematically shown in Fig. 12. The equations for the border points become

$$\begin{aligned} \varphi_o^L(0) &= \psi_S + \theta_{oh} \\ \varphi_o^L(p+1) &= 2\theta_{oh} - \varphi_h^L(p) \\ \varphi_h^L(0) &= \psi_S - \theta_{oh} \\ \varphi_h^L(p+1) &= 2\pi - 2\theta_{oh} - \varphi_o^L(p). \end{aligned} \tag{32}$$

3.4. *Series expansions for the family of Green functions*

We will seek the boundary-value Green functions using the series expansions

$$\begin{aligned} \tilde{D}_o(\varphi_o, \varphi_h) &= [1/\ell \sin(\psi_S - \theta_{oh})] G_o^{(0)}(\varphi_o, \varphi_h) \\ &\quad + (1/\ell) \sum_{n=1}^{\infty} (-u)^n G_o^{(n)}(\varphi_o, \varphi_h) \end{aligned} \tag{33}$$

$$\begin{aligned} \tilde{D}_h(\varphi_o, \varphi_h) &= i\kappa_{ho} G_h(\varphi_o, \varphi_h) \\ &= i\kappa_{ho} \sum_{n=0}^{\infty} (-u)^n G_h^{(n)}(\varphi_o, \varphi_h). \end{aligned} \tag{34}$$

The expansion parameter u is defined in (16). Since we neglect effects due to anomalous scattering, u is a real quantity.

From the Takagi equations (27) and (28), we obtain

$$\partial G_o^{(n)}(\varphi_o, \varphi_h)/\partial\varphi_o = -\sin\varphi_o G_h^{(n-1)}(\varphi_o, \varphi_h), \quad n \geq 1 \tag{35}$$

$$\partial G_h^{(n)}(\varphi_o, \varphi_h)/\partial\varphi_h = \sin\varphi_h G_o^{(n)}(\varphi_o, \varphi_h), \quad n \geq 1, \tag{36}$$

together with

$$\partial G_h^{(0)}(\varphi_o, \varphi_h)/\partial\varphi_h = [\sin\varphi_h/\sin(\psi_S - \theta_{oh})] G_o^{(0)}(\varphi_o, \varphi_h), \quad n = 0.$$

This last equation gives rise to general boundary conditions for those sections of the crystal where first-order scattering is present.

$$G_o^{(0)}(\varphi_o, \varphi_h) = \delta(\varphi_h - (\psi_S - \theta_{oh})) \tag{37}$$

$$G_h^{(0)}(\varphi_o, \varphi_h) = \Theta(\varphi_h - (\psi_S - \theta_{oh})). \tag{38}$$

Θ denotes the Heaviside function. We then obtain the following integral recurrence relations and boundary conditions, from which it becomes possible to calculate the series-expansion coefficients:

$$\begin{aligned} G_o^{(n)}(\varphi_o, \varphi_h|m; r) &= G_o^{(n)}(\varphi_o^b(\varphi_h), \varphi_h|m^b; r) - \int_{\varphi_o^b(\varphi_h)}^{\varphi_o} \mathrm{d}\varphi_o' \\ &\quad \times \sin\varphi_o' G_h^{(n-1)}(\varphi_o', \varphi_h|m; r) \end{aligned} \tag{39}$$

$$\begin{aligned} G_h^{(n)}(\varphi_o, \varphi_h|m; r) &= G_h^{(n)}(\varphi_o, \varphi_h^b(\varphi_o)|m^b; r) + \int_{\varphi_h^b(\varphi_o)}^{\varphi_h} \mathrm{d}\varphi_h' \\ &\quad \times \sin\varphi_h' G_o^{(n)}(\varphi_o, \varphi_h'|m; r) \end{aligned} \tag{40}$$

$G_o^{(0)}(\varphi_o, \varphi_h|m; r) = 0$ in general

$G_h^{(0)}(\varphi_o, \varphi_h^b|m^b; r) = 0$ at the B and C surfaces

$G_h^{(0)}(\varphi_o, \varphi_h|1; \mathsf{B}) = 1$

$G_h^{(0)}(\varphi_o, \varphi_h|m; \mathsf{B}) = 0 \quad m \geq 2$

$G_h^{(0)}(\varphi_o, \varphi_h|1; \mathsf{L}) = 1$

$G_h^{(0)}(\varphi_o, \varphi_h|2; \mathsf{L}) = 1$

$G_h^{(0)}(\varphi_o, \varphi_h|m; \mathsf{L}) = 0 \quad m \geq 3.$

m^b represents a neighbouring region or the crystal boundary.

3.5. *Integration setup*

A nomenclature for the various scattering processes is given in Fig. 13. To determine the coupled ranges of variations for ψ_S and ψ_M, we have to examine the sets of inequalities given in Tables 1 and 2 combined with the constraints given in Table 3. Separate analyses must be performed for the classes of regions $m = 2p+1$ and $m = 2p+2$ in the Bragg scattering situation and for the classes $m = 3p+1$, $m = 3p+2$ and $m = 3p+3$ in the Laue case.

Contributions to the diffracted field at the exit surface A are shown in Fig. 14. The limiting values of θ_{oh}

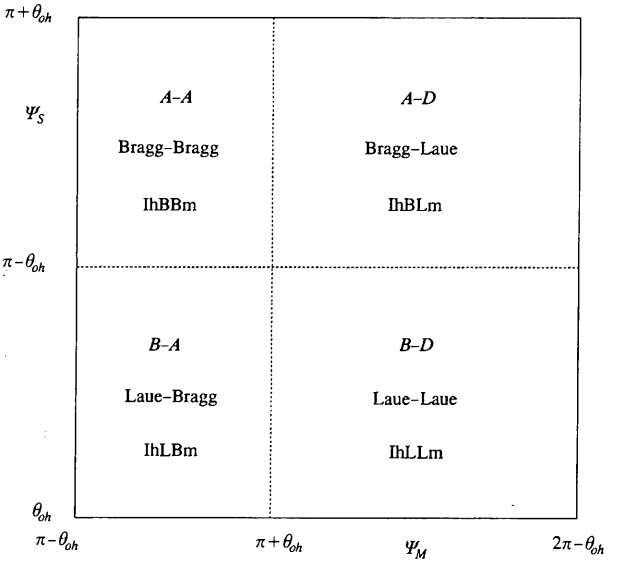

Fig. 13. The scattering processes related to entrance and exit surfaces shown in a (ψ_M, ψ_S) plot. The variables IhLLm, IhBBm, IhLBm and IhBLm are used for the intensity of the diffracted fields in region m. *I.e.* $|G_h(\psi_S, \psi_M|m; \{\mathsf{L}, \mathsf{B}\})|^2$ for the various combinations of entrance and exit surfaces: Laue–Laue, Bragg–Bragg *etc.*

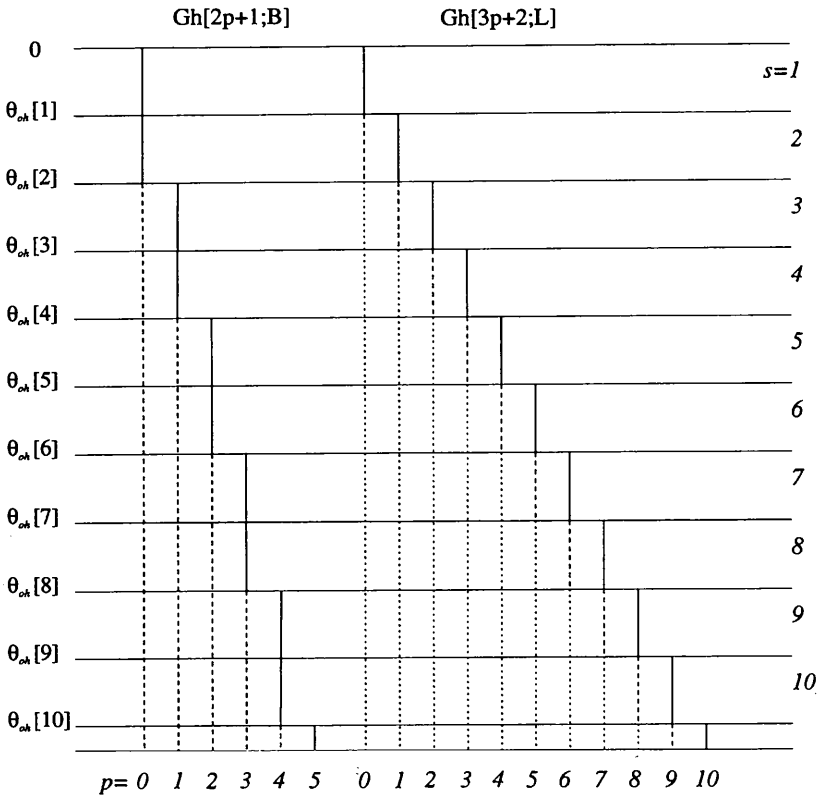

Fig. 14. Contributions to the diffracted field at the exit surface *A*. *s* counts sections in θ_{oh}. Gh[2p + 1; B] = $G_h(\psi_S, \psi_M|m = 2p + 1;$ B), Gh[3p + 2; L] = $G_h(\psi_S, \psi_M|m = 3p + 2;$ L). The solid, dashed and dotted lines represent different integration setups. The illustration indicates the buildup of regions for increasing *s*.

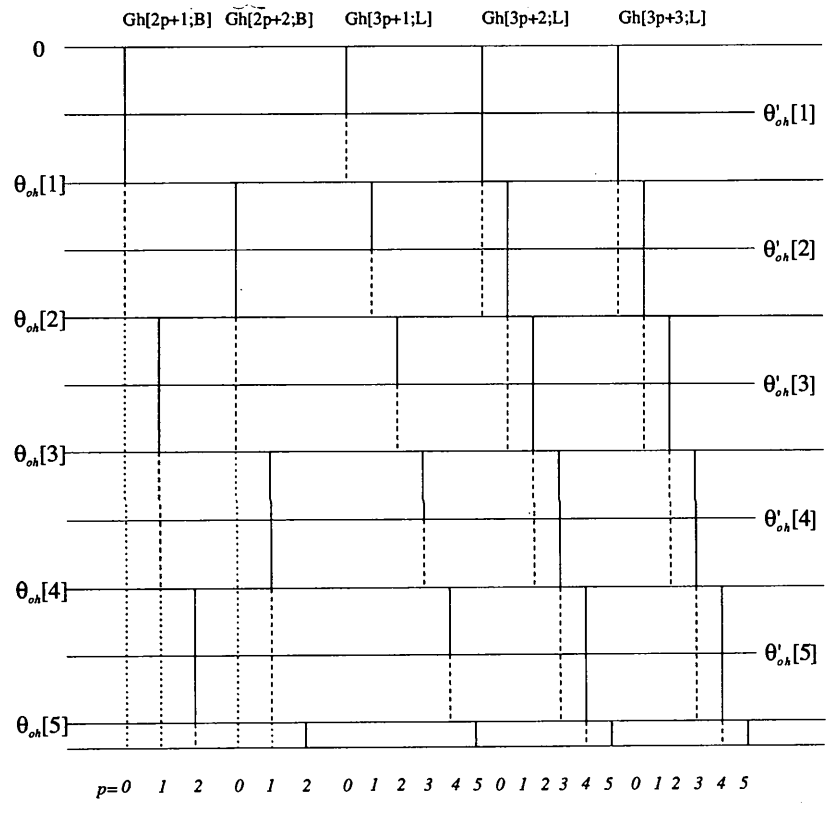

Fig. 15. Contributions to the diffracted field at the exit surface *D*. Nomenclature as in Fig. 14.

Table 1. *Restrictions on the exit point, $(\varphi_o(M), \varphi_h(M))$, associated with a region m in Bragg scattering*

Region	Inequalities
$m = 2p + 1$	$\varphi_o^B(p+1) \le \varphi_o(M) \le \varphi_o^S$ $\varphi_h^B(p) \le \varphi_h(M) \le \varphi_h^B(p+1)$
$m = 2p + 2$	$\varphi_o^B(p+2) \le \varphi_o(M) \le \varphi_o^B(p+1)$ $\varphi_h^S \le \varphi_h(M) \le \varphi_h^B(p+1)$

Table 2. *Restrictions on the exit point, $(\varphi_o(M), \varphi_h(M))$, associated with a region m in Laue scattering*

Region	Inequalities
$m = 3p + 1$	$\varphi_o^L(p+1) \le \varphi_o(M) \le \varphi_o^L(p)$ $\varphi_h^L(p) \le \varphi_h(M) \le \varphi_h^L(p+1)$
$m = 3p + 2$	$\varphi_o^L(p+1) \le \varphi_o(M) \le \varphi_o^S$ $\varphi_h^L(p+1) \le \varphi_h(M) \le \varphi_h^L(p+2)$
$m = 3p + 3$	$\varphi_o^L(p+2) \le \varphi_o(M) \le \varphi_o^L(p+1)$ $\varphi_h^S \le \varphi_h(M) \le \varphi_h^L(p+1)$

Table 3. *Summary of the relations for the various scattering processes, cf. equations (21) and (22) and Fig. 6*

Scattering	ψ_S	ψ_M
A–A	$(\pi - \theta_{oh}, \pi + \theta_{oh})$	$(\pi - \theta_{oh}, \pi + \theta_{oh})$
A–D	$(\pi - \theta_{oh}, \pi + \theta_{oh})$	$(\pi + \theta_{oh}, 2\pi - \theta_{oh})$
B–A	$(\theta_{oh}, \pi - \theta_{oh})$	$(\pi - \theta_{oh}, \pi + \theta_{oh})$
B–D	$(\theta_{oh}, \pi - \theta_{oh})$	$(\pi + \theta_{oh}, 2\pi - \theta_{oh})$

between the different sections are given by the relation

$$\theta_{oh} = \theta_{oh}(s) = [s/(s+1)](\pi/2).$$

Contributions at the exit surface D are shown in Fig. 15. The values of the intermediate limits within the sections are

$$\theta'_{oh} = \theta'_{oh}(s) = [(2s-1)/(2s+1)](\pi/2).$$

The region structure and the limits for the surface integrations are most conveniently shown in a (ψ_M, ψ_S) plot. Two cases within the first section, $0 \le \theta_{oh} \le \pi/4$, are shown in Figs. 16 and 17: $\theta'_{oh}(s)$ is the value of θ_{oh} when the parallelogram associated with the IhLLm field, $m = 3s + 1$, changes orientation.† We have found that the integrated power calculated for the θ_{oh} range $\theta_{oh} \in (\theta_{oh}(s), \theta'_{oh}(s))$ is valid for the entire section, *i.e.* $\theta_{oh} \in (\theta_{oh}(s), \theta_{oh}(s+1))$.

An extensive treatment of the structure of integrations is given by Thorkildsen & Larsen (1997*a*,*b*).

3.6. *Primary extinction – cylinders and spheres*

In this work, we consider a non-absorbing crystal. A new algorithm for calculating absorption and weighted path lengths in cylindrical and spherical crystals, based on surface integrations, will be treated in a following paper (Thorkildsen & Larsen, 1998). Using (30) together with the series expansion for G_h, (34), it turns out that the primary extinction factor can be expressed by

$$y_p = \sum_{n=0}^{n'} (-1)^n f_n^{(s)}(\theta_{oh}) (R/\Lambda_{oh} \sin 2\theta_{oh})^{2n}. \quad (41)$$

The coefficients $f_n^{(s)}(\theta_{oh})$ explicitly depend on the scattering angle θ_{oh} with a separate expression for each section s. n' denotes a practical upper limit in the expansion.

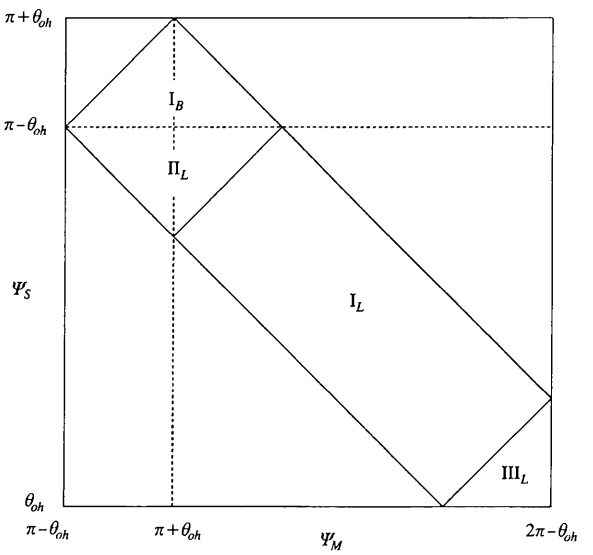

Fig. 16. (ψ_M, ψ_S) plot, $\theta_{oh} = 20° < \theta'_{oh}(0) = 30°$.

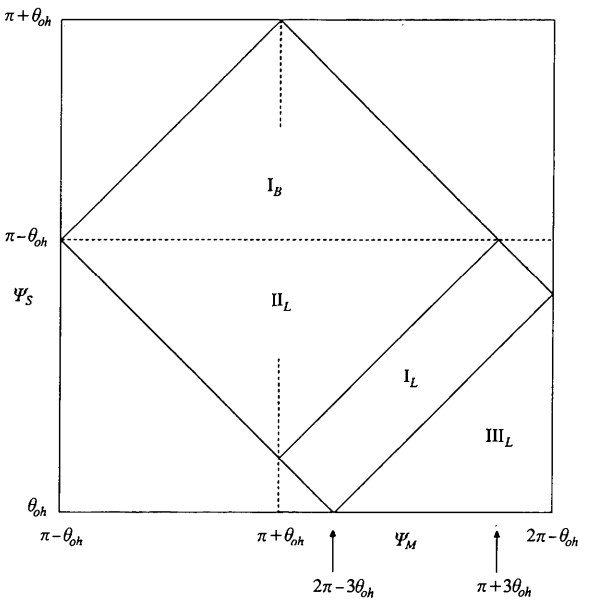

Fig. 17. (ψ_M, ψ_S) plot, $\theta_{oh} = 40° > \theta'_{oh}(0) = 30°$.

† $s = 0$ in Figs. 16 and 17.

The transition from a cylinder to a sphere influences the integration across the vertical dimension of the exit surface only. In (41),

$$R^{2n} \rightarrow R^{2n}(z) \rightarrow R^{2n}(1-z^2)^n$$

and with the shape function, $f(z)$, taken into account, the integration gives

$$\tfrac{3}{2}\int_0^1 \mathrm{d}z\,(1-z^2)^{n+1} = (2)_n/(5/2)_n,$$

where $()_n$ is the Pochhammer symbol (Abramowitz & Stegun, 1965). Thus, (41) applies in both cases with

$$f_n^{(s)(\text{sphere})} = (2)_n/(5/2)_n f_n^{(s)(\text{cylinder})}. \qquad (42)$$

The actual region structures do not depend on $R(z)$ but only on the scattering angle θ_{oh}.

4. Results

4.1. *Primary extinction in a sphere*

It has been possible by the method described here to obtain analytical expressions for the series-expansion coefficients of the primary extinction factor up to fifth order. Owing to the complexity of the terms, we here only present the first-order terms for a sphere. The second-order terms are given in Appendix *A*. *Mathematica* code for the terms up to fifth order is available from the authors on request.

For $0 \le \theta_{oh} \le \pi/4$:

$$y_p = 1 - [(8\sin 2\theta_{oh})/5\pi](1 + \pi\theta_{oh} - 4\theta_{oh}^2 - \cos 4\theta_{oh} - \theta_{oh}\sin 4\theta_{oh})(R/\Lambda_{oh}\sin 2\theta_{oh})^2 + \ldots.$$

For $\pi/4 \le \theta_{oh} \le \pi/2$:

$$y_p = 1 - [(4\sin 2\theta_{oh})/5\pi](2 - \pi^2 + 6\pi\theta_{oh} - 8\theta_{oh}^2 - 2\cos 4\theta_{oh} + \pi\sin 4\theta_{oh} - 2\theta_{oh}\sin 4\theta_{oh}) \times (R/\Lambda_{oh}\sin 2\theta_{oh})^2 + \ldots.$$

According to the literature (Wilkins, 1981; Al Haddad & Becker, 1990), a correct solution for the primary extinction factor should be symmetrical with respect to a reversal of the scattering geometry: $y_p(\theta_{oh}) = y_p(-\theta_{oh})$. By inspecting the above expressions, we find this to be true, bearing in mind that the reversal causes $\pi \rightarrow -\pi$.

Fig. 18 shows the angular dependence of y_p at various values of $x \overset{\text{def}}{=} R/\Lambda_{oh}$ based on the expansion to fifth order. The dots indicate the approximate numerical calculation by Al Haddad & Becker (1990). We note that the extinction factor declines as a function of the Bragg angle up to a certain level, and then rises again. The minimum point seems to be shifted towards lower θ_{oh} values as x increases. The curves are asymmetrical and $y_p(\theta_{oh} = 0°) < y_p(\theta_{oh} = 90°)$.

The Al Haddad & Becker approximation is seen to be very good at small θ_{oh}, but there is a tendency of overestimating the y_p values at high Bragg angles. This reflects the fact that their approximation does not properly cover all the scattering contributions arising as θ_{oh} increases. However, the differences are rather small and their method allows a much greater span in x, which cannot be verified from the present calculations owing to the slow convergence of the series representing y_p. Some numerical results of the calculations for a sphere are shown in Table 4.

By comparing corresponding terms in the series expansion in the limit $\theta_{oh} \rightarrow 0$ with that for a semi-infinite crystal plate, we find for a sphere:

$$y_p(\theta_{oh} \rightarrow 0) = \sum_{n=0}^{\infty}\left\{(3\times 4^n)\Big/\left[(2n+1)(2n+3)\prod_{k=2}^{n}k^2\right]\right\}x^{2n} = {}_1F_2[\tfrac{1}{2};1,\tfrac{5}{2};-4x^2]; \qquad (43)$$

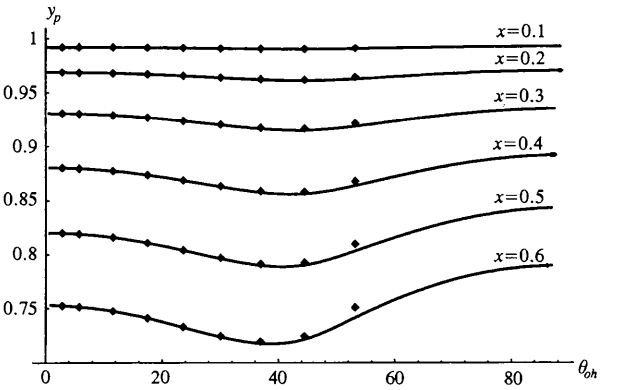

Fig. 18. Angular dependence of the primary extinction factor in a sphere. Marks indicate the approximative numerical calculations by Al Haddad & Becker. $x = R/\Lambda_{oh}$. With five terms only in the series expansion for y_p, a rather limited range in x is covered.

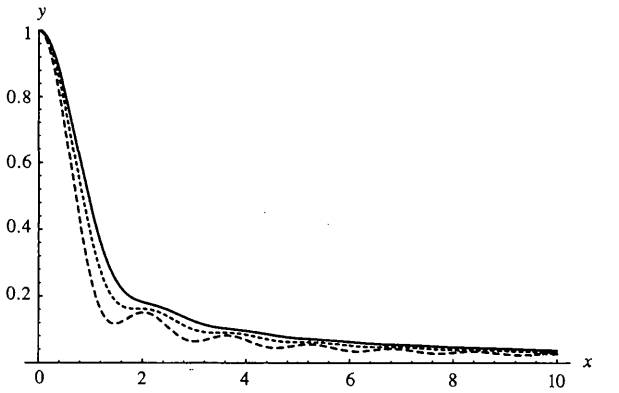

Fig. 19. Primary extinction factor curves at $\theta_{oh} = 0$ as a function of x. Solid line: sphere; dotted line: cylinder; dashed line: slab.

Table 4. *Primary extinction factor for a spherical crystal*

The absolute error in the calculated quantities is less than 2×10^{-4}.

x	$\theta_{oh} = 0°$	10°	20°	30°	40°	50°	60°	70°	80°	90°
0.0	1	1	1	1	1	1	1	1	1	1
0.1	0.9920	0.9919	0.9914	0.9908	0.9900	0.9900	0.9907	0.9914	0.9919	0.9921
0.2	0.9685	0.9679	0.9661	0.9633	0.9609	0.9612	0.9640	0.9669	0.9688	0.9694
0.3	0.9307	0.9294	0.9254	0.9198	0.9151	0.9165	0.9230	0.9292	0.9333	0.9347
0.4	0.8804	0.8782	0.8718	0.8629	0.8562	0.8602	0.8719	0.8825	0.8892	0.8915
0.5	0.8202	0.8170	0.8081	0.7962	0.7887	0.7975	0.8156	0.8306		
0.6	0.7527	0.7487	0.7376	0.7237	0.7175	0.7332				
0.7	0.6811	0.6764	0.6638	0.6495	0.6470					
0.8	0.6084	0.6033	0.5901	0.5772						
0.9	0.5373	0.5322								

and similarly for a cylinder:

$$y_p(\theta_{oh} \to 0) = {}_1F_2[\tfrac{1}{2}; 1, 2; -4x^2]. \qquad (44)$$

${}_pF_q[a; b, c; z]$ is a *generalized hypergeometric function* (Abramowitz & Stegun, 1965). In Fig. 19, we have shown the results for the primary extinction factor in this limit for a sphere, a cylinder and a semi-infinite crystal slab (Zachariasen, 1945, 1967) with thickness $2R$. We observe that the *Pendellösung* oscillations are most prominent for the slab, whereas they are barely visible in the spherical case. It is also to be noted that $y_p^{(\text{sphere})} > y_p^{(\text{cylinder})} > y_p^{(\text{slab})}$ for every x. This is expected, taking into consideration the different distributions of path lengths within the various crystal geometries.

4.2. *Expansion coefficients – asymptotic behaviour*

The coefficients $f_n^{(s)}(\theta_{oh})$ are depicted in Fig. 20. They are continuous across the different borders in s. We find that the maxima of the curves decrease and shift towards higher θ_{oh} values as n increases. The lowest orders in the series expansions are $n = m/2$ within the Bragg family and $n = (m+3)/6$ within the Laue family (integer division). Then, by examining Figs. 9 and 11 and relating their structures to that of a (ψ_M, ψ_S) plot, it becomes apparent that there will be an asymptotic limit for $f_n^{(s)}$, *i.e.* an upper value for s, $s_{\max}(n)$, beyond which no new contributions to the integrated power are generated to the order n. This should occur for

$$s_{\max} = n + 2, \qquad n \text{ odd}$$
$$s_{\max} = n + 3, \qquad n \text{ even}.$$

In practice, we always find the asymptotic limit for $s = s_{\max} - 1$. Fig. 21 shows the contributions to the coefficient f_1 for the different scattering processes.

We note the following features:

(i) The curves are all asymmetrical but continuous.

(ii) The derivative of the IhLL2 curve is not continuous at $\theta_{oh} = 45°$. This is in accordance with Werner *et al.* (1966) who pointed out that the diffracted fields, but not their derivatives, had to be continuous at the region borders.

(iii) The mixed contributions (IhLB2 and IhBL1) are equal. It seems that $\mathcal{P}_h^{(A-D)} = \mathcal{P}_h^{(B-A)}$ represents a general symmetry property of the power contributions for this crystal geometry. It is found that the contributions are equal about the diagonal line $\psi_S = -\psi_M + 2\pi$ in the (ψ_M, ψ_S) plot, *i.e.* IhBL$[m = 2p + 1]$ = IhLB$[m = 6p + 2]$ and IhBL$[m = 2p + 2]$ = IhLB$[m = 6p + 5]$.

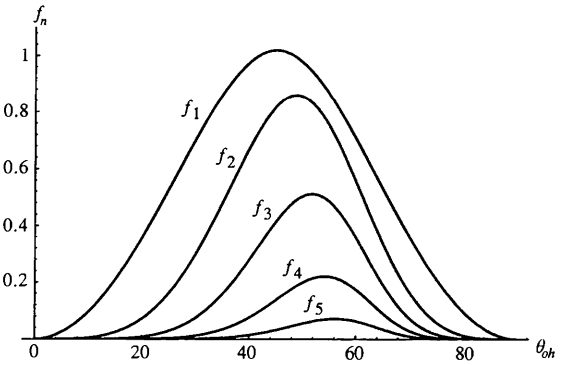

Fig. 20. First- to fifth-order expansion coefficients for the primary extinction factor in a sphere.

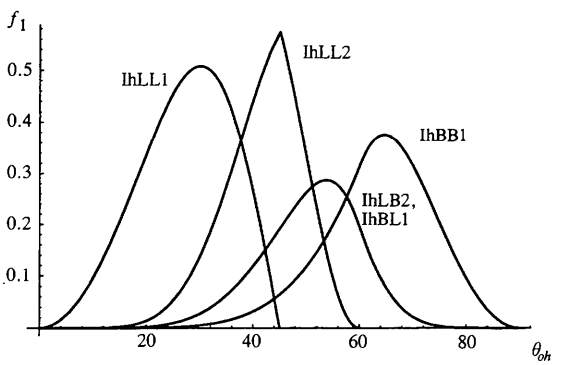

Fig. 21. Contributions from the various scattering modes at the exit surface to the coefficient f_1 of a spherical crystal.

5. Conclusions

The calculations of the coefficients for the primary extinction factor are very time and memory consuming. They were performed on a PC equipped with a 90 MHz Pentium processor and 64 Mbyte of RAM. The fifth-order term represents the upper limit accessible with respect to both the hardware and the software.

The use of numerical methods would be a way to extend the range of (θ_{oh}, x) for which values for the primary extinction factor could be calculated. However, based on the results presented in Fig. 18, this will give little new compared with the approximative treatment of Al Haddad & Becker (1990).

It will perhaps be more interesting, from a theoretical point of view, to adopt the method of solving Takagi's equations presented by Werner *et al.* (1966) to the angular representation of these equations, (27) and (28).

APPENDIX *A*
Expansion coefficients $f_2^{(s)}$, $s = 1$–3

We here present the second-order expansion coefficients for the primary extinction factor. The asymptotic level is reached for $s = 3$.

$s = 1$ or $0 \le \theta_{oh} \le \pi/4$:

$$\begin{aligned} f_2^{(1)} = (\sin 2\theta_{oh}/105\pi)(&512 - 212\cos 2\theta_{oh} \\ &- 216\pi\theta_{oh}\cos 2\theta_{oh} + 864\theta_{oh}^2\cos 2\theta_{oh} \\ &- 512\cos 4\theta_{oh} + 217\cos 6\theta_{oh} - 5\cos 10\theta_{oh} \\ &+ 108\pi\sin 2\theta_{oh} - 1248\theta_{oh}\sin 2\theta_{oh} \\ &+ 138\theta_{oh}\sin 6\theta_{oh} - 6\theta_{oh}\sin 10\theta_{oh}). \end{aligned} \tag{45}$$

$s = 2$ or $\pi/4 \le \theta_{oh} \le \pi/3$:

$$\begin{aligned} f_2^{(2)} = (\sin 2\theta_{oh}/105\pi)(&512 + 337\cos 2\theta_{oh} \\ &- 324\pi^2\cos 2\theta_{oh} + 2304\pi\theta_{oh}\cos 2\theta_{oh} \\ &- 4032\theta_{oh}^2\cos 2\theta_{oh} - 512\cos 4\theta_{oh} - 432\cos 6\theta_{oh} \\ &+ 216\pi^2\cos 6\theta_{oh} - 1512\pi\theta_{oh}\cos 6\theta_{oh} \\ &+ 2592\theta_{oh}^2\cos 6\theta_{oh} + 72\cos 10\theta_{oh} + 22\cos 14\theta_{oh} \\ &+ \cos 18\theta_{oh} - 744\pi\sin 2\theta_{oh} + 216\pi^3\sin 2\theta_{oh} \\ &+ 2250\theta_{oh}\sin 2\theta_{oh} - 2304\pi^2\theta_{oh}\sin 2\theta_{oh} \\ &+ 8064\pi\theta_{oh}^2\sin 2\theta_{oh} - 9216\theta_{oh}^3\sin 2\theta_{oh} \\ &+ 489\pi\sin 6\theta_{oh} - 1728\theta_{oh}\sin 6\theta_{oh} - 39\pi\sin 10\theta_{oh} \\ &+ 144\theta_{oh}\sin 10\theta_{oh} - 12\pi\sin 14\theta_{oh} \\ &+ 42\theta_{oh}\sin 14\theta_{oh}). \end{aligned} \tag{46}$$

$s = 3$ or $\pi/6 \le \theta_{oh} \le 3\pi/8$. The result is valid for the entire range $\pi/6 \le \theta_{oh} \le \pi/2$.

$$\begin{aligned} f_2^{(3)} = (\sin 2\theta_{oh}/105\pi)(&-95\cos 2\theta_{oh} + 180\pi^2\cos 2\theta_{oh} \\ &- 936\pi\theta_{oh}\cos 2\theta_{oh} + 1152\theta_{oh}^2\cos 2\theta_{oh} \\ &+ 81\cos 6\theta_{oh} + 9\cos 10\theta_{oh} + 5\cos 14\theta_{oh} \\ &+ 108\pi\sin 2\theta_{oh} - 72\pi^3\sin 2\theta_{oh} - 342\theta_{oh}\sin 2\theta_{oh} \\ &+ 576\pi^2\theta_{oh}\sin 2\theta_{oh} - 1440\pi\theta_{oh}^2\sin 2\theta_{oh} \\ &+ 1152\theta_{oh}^3\sin 2\theta_{oh} - 123\pi\sin 6\theta_{oh} \\ &+ 216\theta_{oh}\sin 6\theta_{oh} - 18\pi\sin 10\theta_{oh} + 36\theta_{oh}\sin 10\theta_{oh} \\ &- 3\pi\sin 14\theta_{oh} + 6\theta_{oh}\sin 14\theta_{oh}). \end{aligned} \tag{47}$$

Parts of this work have been presented at the International School of Crystallography, 23rd Course. X-ray and Neutron Dynamical Diffraction: Theory and Applications, Erice, Italy, 1996.

References

Abramowitz, M. & Stegun, I. (1965). *Handbook of Mathematical Functions*. New York: Dover.

Al Haddad, M. & Becker, P. (1990). *Acta Cryst.* A**46**, 112–123.

Authier, A. (1996*a*). *International Tables for Crystallography*, Vol. B, edited by U. Shmueli, pp. 464–480. Dordrecht: Kluwer Academic Publishers.

Authier, A. (1996*b*). *Proceedings of X-ray and Neutron Dynamical Diffraction: Theory and Applications*, NATO ASI Series, Series B: Physics, Vol. 357, edited by A. Authier, S. Lagomarsino & B. Tanner, pp. 43–62. New York: Plenum.

Authier, A. & Simon, D. (1968). *Acta Cryst.* A**24**, 517–526.

Batterman, B. W. & Cole, H. (1964). *Rev. Mod. Phys.* **36**, 681–717.

Becker, P. (1977). *Acta Cryst.* A**33**, 667–671.

Becker, P. (1983). *Acta Cryst.* A**39**, 89–90.

Becker, P. & Coppens, P. (1974*a*). *Acta Cryst.* A**30**, 129–147.

Becker, P. & Coppens, P. (1974*b*). *Acta Cryst.* A**30**, 148–153.

Becker, P. & Dunstetter, F. (1984). *Acta Cryst.* A**40**, 241–251.

Char, B. W., Geddes, K. O., Gonnet, G. H., Leong, B. L., Monagan, M. B. & Watt, S. M. (1991*a*). *Maple V Language Reference Manual*. New York: Springer-Verlag.

Char, B. W., Geddes, K. O., Gonnet, G. H., Leong, B. L., Monagan, M. B. & Watt, S. M. (1991*b*). *Maple V Library Reference Manual*. New York: Springer-Verlag.

Darwin, C. G. (1914). *Philos. Mag.* **27**, 675–690.

Darwin, C. G. (1922). *Philos. Mag.* **43**, 800–829.

Ekstein, H. (1951). *Phys. Rev.* **83**(4), 721–729.

Ewald, P. P. (1917). *Ann. Phys. (Leipzig)*, **54**, 519–597.

Hamilton, W. C. (1957). *Acta Cryst.* **10**, 629–634.

Härtwig, J. (1987). *Acta Cryst.* A**43**, 522–525.

Jackson, J. D. (1975). *Classical Electrodynamics*. New York: John Wiley.

Kato, N. (1976*a*). *Acta Cryst.* A**32**, 453–457.

Kato, N. (1976*b*). *Acta Cryst.* A**32**, 458–466.

Kato, N. (1980*a*). *Acta Cryst.* A**36**, 171–177.

Kato, N. (1980*b*). *Acta Cryst.* A**36**, 763–769.

Kato, N. (1980*c*). *Acta Cryst.* A**36**, 770–778.

Kato, N. (1980*d*). *Electron and Magnetization Densities in Molecules and Crystals*, NATO ASI Series, Series B: Physics, Vol. 48, edited by P. Becker, pp. 237–253. New York: Plenum.

Kawamura, T. & Kato, N. (1983). *Acta Cryst.* A**39**, 305–310.

Laue, M. von (1932). *Ergeb. Exakten Naturwiss.* **10**, 133–158.
Olekhnovich, N. M. & Olekhnovich, A. I. (1978). *Acta Cryst.* A**34**, 321–326.
Olekhnovich, N. M. & Olekhnovich, A. I. (1980). *Acta Cryst.* A**36**, 22–27.
Pinsker, Z. G. (1978). *Dynamical Scattering of X-rays in Crystals.* Berlin: Springer-Verlag.
Saka, T., Katagawa, T. & Kato, N. (1972*a*). *Acta Cryst.* A**28**, 102–113.
Saka, T., Katagawa, T. & Kato, N. (1972*b*). *Acta Cryst.* A**28**, 113–120.
Saka, T., Katagawa, T. & Kato, N. (1973). *Acta Cryst.* A**29**, 192–200.
Sneddon, I. N. (1957). *Elements of Partial Differential Equations.* London: McGraw-Hill.
Sommerfeld, A. (1949). *Partial Differential Equations.* New York: Academic Press.
Takagi, S. (1962). *Acta Cryst.* **15**, 1311–1312.
Takagi, S. (1969). *J. Phys. Soc. Jpn*, **26**, 1239–1253.
Taupin, D. (1964). *Bull. Soc. Fr. Minéral. Cristallogr.* **87**, 469–511.
Thorkildsen, G. & Larsen, H. B. (1997*a*). *Two Beam Diffraction in Perfect Crystals Analyzed by Takagi's Equations.* Part 1. *Basic Principles and Methods of Solution.* Technical Report 30. Stavanger College, Stavanger, Norway.
Thorkildsen, G. & Larsen, H. B. (1997*b*). *Two Beam Diffraction in Perfect Crystals Analyzed by Takagi's Equations.* Part 2. *Function Definitions, Notebooks and Worksheets.* Technical Report 31. Stavanger College, Stavanger, Norway.
Thorkildsen, G. & Larsen, H. B. (1998). *Acta Cryst.* A**54**, 186–190.
Uragami, T. S. (1969). *J. Phys. Soc. Jpn*, **27**, 147–154.
Uragami, T. S. (1970). *J. Phys. Soc. Jpn*, **28**, 1508–1527.
Uragami, T. S. (1971). *J. Phys. Soc. Jpn*, **31**, 1141–1161.
Weiss, R. G. (1952). *Proc. R. Soc. London Ser. B*, **65**, 553–555.
Werner, S. (1974). *J. Appl. Phys.* **45**, 3246–3254.
Werner, S. A. & Arrott, A. (1965). *Phys. Rev.* **140**, 675–686.
Werner, S. A., Arrott, A., King, J. S. & Kendrick, H. (1966). *J. Appl. Phys.* **37**, 2343–2350.
Werner, S. A., Berliner, R. R. & Arif, M. (1986). *Physica (Utrecht)*, **137**B, 245–255.
Wilkins, S. W. (1981). *Philos. Trans. R. Soc. London*, **299**, 275–317.
Wolfram, S. (1991). *Mathematica – A System for Doing Mathematics by Computer.* New York: Addison-Wesley.
Zachariasen, W. H. (1945). *Theory of X-ray Diffraction in Crystals.* London: John Wiley.
Zachariasen, W. H. (1963). *Acta Cryst.* **16**, 1139–1144.
Zachariasen, W. H. (1967). *Acta Cryst.* **23**, 558–564.